Simulation of the Atlantic Circulation with a Coupled Sea Ice–Mixed Layer–Isopycnal General Circulation Model. Part II: Model Experiment

JOSEF M. OBERHUBER*

Meteorologisches Institut der Universität Hamburg, Hamburg, Germany

(Manuscript received 8 July 1991, in final form 18 May 1992)

ABSTRACT

An ocean general circulation model (OGCM) formulated on isopycnal coordinates is used to model the circulation of the Atlantic. The model domain is bounded meridionally at 30°S and the North Pole and extends zonally from 100°W to 50°E with cyclic boundary conditions in the Arctic basin. The Atlantic sector of the Arctic basin is included in order to obtain a more realistic exchange of water masses between the North Atlantic and the Arctic. For the purpose of achieving a sufficient resolution of the high-latitude current systems, the grid spacing is made variable with a 2° × 2° resolution in the entire equatorial and North Atlantic and a steadily increasing resolution in the Greenland–Iceland–Norwegian seas towards about 1° zonally and 0.5° meridionally. The model is integrated over 100 years, with acceleration of the deeper layers during the first 50 years. Initial conditions are observed annual mean temperature and salinity. After the adjustment period the ocean approaches a cyclo-stationary state, except for the deep ocean where temperature and salinity have not become stationary.

The model yields realistic equatorial currents and also simulates the separation of the Gulf Stream and the complex current structure in the Greenland–Iceland–Norwegian seas. Heat and freshwater fluxes and the seasonal variation of the mixed-layer depth agree reasonably with observations. The stratification of the upper ocean demonstrates the capability of an isopycnal model with thermodynamics to reproduce the thermohaline circulation. Finally, the simulated sea ice cover is considered in order to discuss the coupling among sea ice, mixed layer, and the deep ocean.

1. Introduction

The goal of this study is to demonstrate that the very limited period of use of isopycnal models of the ocean or isentropic models for the atmosphere approaches its end. The restrictions due to insufficient techniques to treat Lagrangian coordinates in conjunction with an arbitrary topography or to include a complex equation of state have been the major reasons for the slow development in the past. Furthermore, while atmospheric models with isentropic coordinates can use the simplicity of the equation of state for dry air to introduce the Montgomery potential and to transform the set of equations, this is not possible for the ocean as the equation of state has to be used as black box due to its complexity. Naturally, the main purpose of such types of ocean models is the treatment of the circulation in the thermocline as detrained surface water propagates by force along the chosen coordinates toward the correct location. Regions of low stability are naturally resolved less well, as in z-coordinate models. With respect to wave physics this is not severe since the barotropic mode dominates in this case. The number of available layers adjusts to the number of modes necessary to treat wave propagation. However, advective phenomena in neutrally stratified areas will possibly not be resolved sufficiently in the vertical. Therefore, isopycnal models will a priori have difficulties to reproduce the deep overturning essential for long climate runs. On the other hand, z-coordinate models a priori have problems with the thermocline, which, for example, can be reduced by rotating the diffusion operator as proposed by Redi (1982) and McDougal and Church (1986) but cannot be removed totally like other discretization errors, such as concerning advection, which cannot be treated exactly in the same manner. Such methods are superfluous in isopycnal models. Features such as wave propagation and tracer advection in the upper ocean are treated in a more natural way. This was demonstrated by Miller et al. (1991) who used an early release of this model for El Niño studies.

As a first test area it is obvious to choose the Atlantic Ocean, since it is one of the oceans with the best data coverage and contains many of those features relevant for the mean state of the global ocean and consequently for the earth's climate. Features such as equatorial currents, western boundary currents or eddy activity (with their importance to meridional heat transport), various

* Permanent affiliation: Max-Planck-Institut für Meteorologie, Germany.

Corresponding author address: Dr. Joseph M. Oberhuber, Max-Planck-Institut für Meteorologie, Bundesstrasse 55, D-2000 Hamburg 13, Germany.

upwelling regimes, the effects of sea ice or topography on the ocean state, or the role of the deep-water formation can all be studied in a limited domain. To some extent, the results must be considered with caution since many quantities, such as meridional overturning, meridional heat transport, or the water mass distribution in the deep Atlantic are highly dependent on the boundary conditions chosen to shut off the remaining global ocean. However, experiments can be run at relatively low computing costs compared with those performed with a global model. Atlantic studies have been carried out by Holland and Hirschman (1972), who used the first version of the primitive equation model of Bryan (1969), and more recently by Sarmiento (1986), who used an improved version of the GFDL model to study the heat storage. Lately, Killworth et al. (1991) tested their free-surface version of the model of Cox (1984) on a coarse-grid Atlantic. Bleck and Boudra (1986) developed a wind-driven pure isopycnic coordinate model, which was adapted by Smith (1987) to the Atlantic. Also the Numerical Experimentation Group of the World Ocean Circulation Experiment (WOCE-NEG) carried out model comparisons for the Atlantic as preparation for the investigation of the global ocean, which are now under consideration also. Meanwhile even eddy-resolving experiments for the North Atlantic as performed by Bryan and Holland (1989) or Böning et al. (1991) with the so-called Community Model (provided by NCAR) are used to resolve, at least partly, effects due to eddy heat transport explicitly.

Meanwhile, Bleck's group (Miami) is on the threshold of completing an OGCM based on isopycnal coordinates. However, the underlying strategy as well as the purpose of both models is slightly contrary. While this model is developed towards a large scale, potentially global, Bleck's ocean model currently tends toward regional models. This governs the choice of techniques. For instance, Bleck uses explicit time integration schemes that are doubtless superior when eddy-resolving phenomena should be investigated. In contrast, this model uses implicit techniques with the advantages that variability on longer time scales or the stability problems in spherical coordinates at high latitudes can be treated more economically.

This paper is structured as follows. The model is briefly described in section 2, and the employed model forcing is outlined in section 3. Section 4 contains the description of the numerical results: first, the model's layout is defined in section 4a, then the simulated general circulation is described in section 4b in terms of flow patterns, horizontal and meridional overturning streamfunctions, and sea surface elevation, followed by a discussion of the relation between surface fluxes and the response in the upper ocean in section 4c. Subsequently, the simulation of the mixed layer and its relation to other upper-ocean quantities (section 4d) are examined. Using meridional cross sections of temperature, salinity, potential density, and layer thickness distribution (section 4e), it is demonstrated that a model with isopycnic coordinates is able to simulate a quite realistic thermocline. Finally, results from the sea ice model are discussed briefly in section 4f in order to illustrate that the model will be used as a global circulation model.

2. The ocean model

The ocean model is described in detail in Part I (Oberhuber 1993) of this paper. In summary, the model consists of four components: A model for the deep ocean that uses isopycnal coordinates, an actively coupled mixed-layer model, a sea ice model with rheology, and detailed flux parameterizations. The ocean itself is formulated with primitive equations in flux form. Due to the use of isopycnals as vertical coordinates it is natural to write the equations as prognostic equations for layer thicknesses, the distance of two isopycnals. Thus, the prognostic variables are the integrals of mass flux, mass, heat, and salt over the column bounded by two interfaces. A realistic equation of state is used to relate density with temperature and salinity as well as temperature with potential temperature and potential density. The mixed-layer model is based on the assumption that turbulent kinetic energy is dissipated within a length scale determined by the Ekman-layer thickness. A similar assumption holds for the buoyancy flux. Solar radiation is allowed to penetrate through the surface and is absorbed below the surface determined by given water properties. Further parameterizations for vertical mixing, convection, and the sea ice–mixed layer coupling are introduced. The sea ice model is written in flux form for the ice thickness, ice concentration, and ice flow as prognostic variables. Besides the thermodynamical forcing a viscous-plastic rheology as well as a lead parameterization are included.

The model is formulated on spherical coordinates. On the isopycnals, which run essentially in the horizontal, the discretization is based on a staggered grid while vertically the prognostically determined interface heights represent Lagrangian coordinates. The time stepping scheme is a combination of the semi-implicit technique and a predictor–corrector scheme. Besides the conservation of mass, heat, and salt that are ensured through the use of the flux form, a potential vorticity conserving scheme is included to formulate the momentum transport.

3. Model forcing

The surface fluxes used to force the model are the fluxes of momentum, heat, fresh water, turbulent kinetic energy, and buoyancy. Required datasets are surface air temperature, sea surface temperature, relative humidity, cloudiness, the time-averaged absolute wind speed and its standard deviation, wind stress, rainfall, and surface salinity. Except for the annual-mean sur-

face salinity, the data are monthly mean climatological values. The flux of momentum is taken from Hellermann and Rosenstein (1983). Based on the COADS (Comprehensive Ocean–Atmosphere Data Set; Woodruff et al. 1987), Wright (1988) prepared data on a 2° × 2° grid, which is sufficiently fine for forcing an OGCM. The climatology covers the years 1950–79. From this data source Oberhuber (1988) derived all fluxes required for forcing the ocean model such as heat, buoyancy, fresh water, and turbulent kinetic energy. In regions for which only insufficient data are available from the COADS, spatially complete fields are constructed by overlapping fields of other authors and smoothing the transition zones. For instance, the air temperature over sea ice is taken from Shea (1986).

4. Numerical results

The first experiment with this new type of model represents an attempt to describe the climatological seasonal cycle of the Atlantic Ocean in terms of extreme summer and winter conditions. The analysis of the experiment encompasses the evaluation of the surface fluxes, the mixed layer, the sea ice, and the deep ocean represented by isopycnic coordinates. Despite its small extent, many processes are acting in the Atlantic, which are believed to be of general importance for the circulation of the world ocean. Specifically, questions of general concern are discussed; for example, how the deep ocean is fed by convection and alongisopycnal transport, whether the model is able to reproduce the Gulf Stream separation at Cape Hatteras and the splitting in the central North Atlantic and how the results are related to properties of the chosen coordinates and techniques.

a. Layout of the Atlantic model

The model domain extends from 30°S to 90°N. The southern boundary is an artificial wall at a latitude of an assumed small meridional heat transport and where it does not essentially disturb the subtropical gyre south of the equator. The Antarctic Intermediate and Antarctic Bottom water intruding from the Southern Hemisphere will be cut off by the southern boundary. The northern boundary is the North Pole. The basin extends from 100°W to 50°E with a cyclic boundary condition in the Arctic.

The horizontal resolution is variable. The model uses a 2° × 2° resolution in the equatorial and North Atlantic and an increased resolution in the Greenland–Iceland–Norwegian seas where the grid spacing decreases to 1° zonally and 0.5° meridionally. This results in a resolution of about 50 km there. To keep the grid orthogonal and rectilinear, the zonal grid achieves the highest resolution around Greenwich and decays to the 2° grid within a bandwidth of 20° to the east and to the west of Greenwich. The meridional grid has its highest resolution at 60°N and decays to a 2° grid within a band of 10° to the south and to the north. Splines ensure a smooth transition between regions of low and high resolution to avoid computational modes. This spatially variable grid is sufficiently fine to resolve the large-scale circulation in the North Atlantic basin. It also accounts for the complex current structure around Iceland. Thereby, the enhanced resolution has the task of promoting the development of the water masses on scales that control, for example, the production of deep heavy water by convection, and therefore is of relevance for the whole Atlantic Ocean.

Only nine layers in the vertical were taken to test whether this rather coarse vertical resolution is sufficient to resolve the vertical stratification. Eight of these layers are isopycnic. Their prescribed potential densities are 23.915, 24.782, 25.561, 26.247, 26.834, 27.314, 27.679, and 27.844 in σ units for the second to the deepest layer. These values were chosen to describe the thermal structure with equal temperature differences at each interface for an average salinity value. The initial layer thicknesses are derived from Levitus (1982) by searching the interfaces in such a way that the integral of temperature and salinity transformed into potential density coincides with the prescribed potential density.

The control run is carried out over 100 years, with the first 50 years accelerated. The final 50 years are not accelerated to avoid any influence of errors on the final results due to the acceleration technique. Starting from the second layer, the acceleration coefficient is linearly increased towards a value of 10 in the deepest layer. The time step is 2 days, which gives an effective time step for the deepest layer of 20 days.

The topography is a smoothed version of Lee and Kaula (1967). Figure 1 shows the bottom topography together with the coastline geometry. The Mediterra-

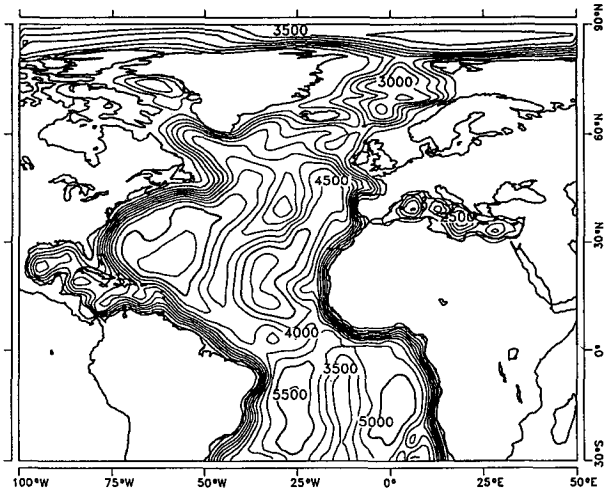

FIG. 1. Bottom topography used in the Atlantic model. Contour interval is 500 m, the thick line marks a depth of 5000 m. The real coastline geometry is indicated by a thick line.

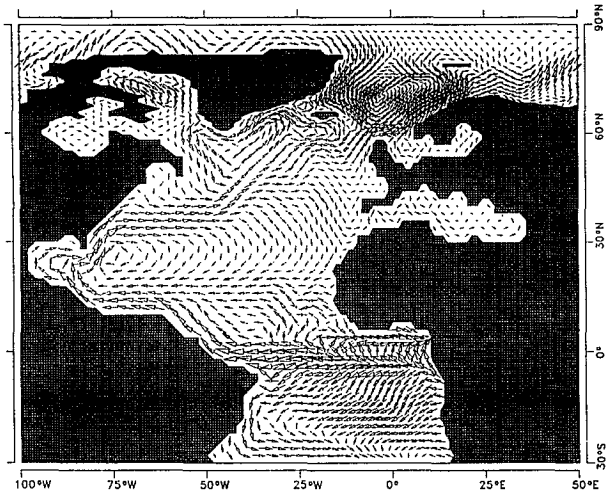

FIG. 2. Surface (mixed layer) flow field for February. Length of velocity vector is proportional to the square root of the velocity. Typical velocities are 50 cm s^{-1} in the equatorial current and 20–30 cm s^{-1} in the Gulf Stream. Only each second vector is plotted.

nean Sea is part of the model, but owing to the insufficient resolution, the flow through the Gibraltar Strait will be underestimated; thus, the salty tongue extending into the deep Atlantic cannot be maintained.

b. Basic quantities of the Atlantic circulation

In the following description, February and August are selected as the most extreme winter and summer months. Figure 2 shows the surface currents for February. A well-developed Gulf Stream appears with a maximum velocity of 35 cm s^{-1} at the American coast. The Gulf Stream separates from the North American coast and then propagates northeastward. In the central North Atlantic it splits into two branches, one propagating northeastward and the other returning into the subtropics. This diffusive splitting occurs east of the highest elevation of the Mid-Atlantic ridge. The North Atlantic Current penetrates into the Norwegian Sea, continues as a coastal current, and then splits into two branches, one propagating into the Barents Sea and the other continuing in a cyclonic gyre in the Greenland–Iceland–Norwegian seas. The other branch of the North Atlantic current turns northwestward at about the Faroe Islands (which are not explicitly resolved by the model grid), passes Iceland, enters the Davis Strait as the Greenland Current, continues as a well-pronounced southward-moving Labrador Current, and finally ends in the Gulf Stream.

Olbers et al. (1985) used the β-spiral technique to determine the circulation in midlatitudes from hydrographic data. Their analysis of observed data for the flow at 100-m depth (Fig. 3), or the more detailed analysis based on observations of the North Atlantic Current provided by Krauss (1986), shows a good cor-

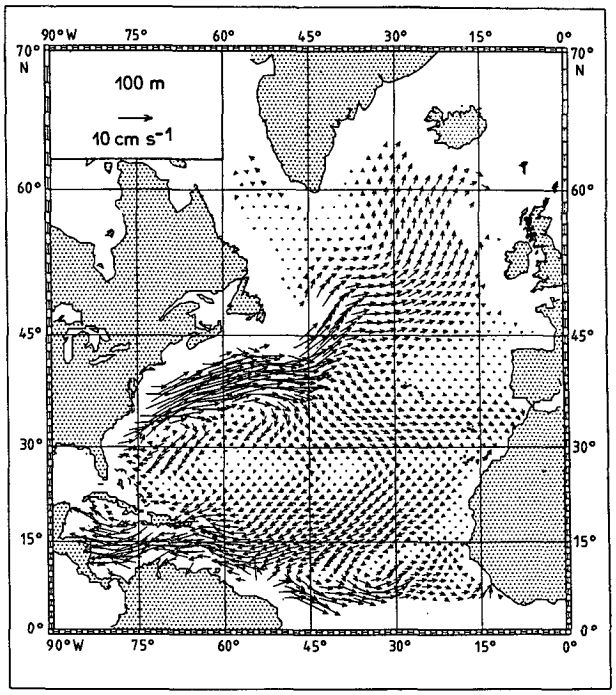

FIG. 3. Flow field at 100-m depth derived from Olbers et al. (1985) from hydrographic data using the β-spiral method.

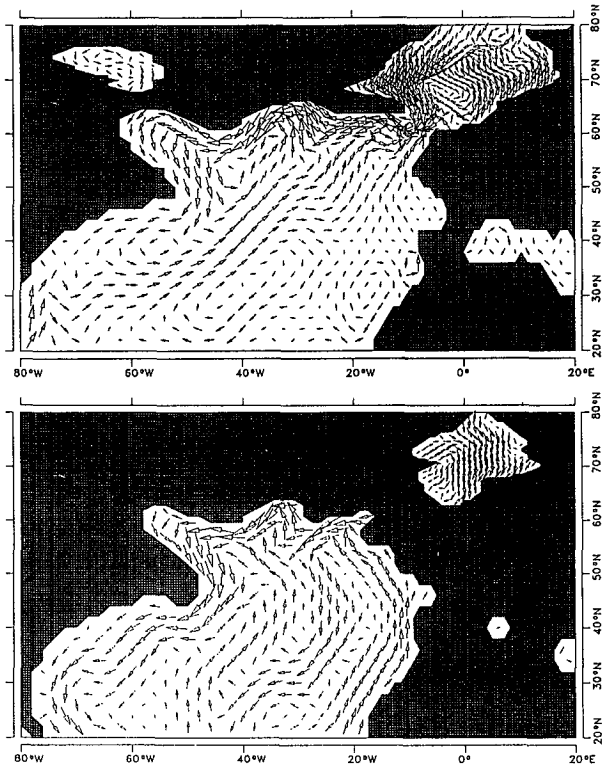

FIG. 4. Upper panel (a) shows the flow field in August for 750-m depth and lower panel (b) the flow field at 2000-m depth. Length of velocity vector is proportional to the square root of the velocity; every second vector plotted. Maximal velocity for (a) is about 10 cm s^{-1} and for (b) about 5 cm s^{-1}.

respondence with the simulation. In terms of the surface flow, it is evident that the simulated Gulf Stream is too weak. This is presumably due to the coarse resolution, which causes the Ekman drift to conceal patterns belonging to the Gulf Stream. Also it separates too late; however, this is compensated by too zonal eastward propagation. Descending into the deep ocean, Figs. 4a,b show the currents at 250-m and 2000-m depth. Compared with the surface flow it is evident that the subtropical gyre weakens with depth. But the outflow of water from the Norwegian Sea into the North Atlantic intensifies with depth. The current propagates westward along the bottom slope of Iceland and Greenland. At 2000 m (where a direct connection between the two basins no longer exists) this current propagates southward as an undercurrent into the Gulf Stream area and ends in the Southern Hemisphere (not shown, since this result is meaningless due to the closed southern boundary). In the deep ocean it is also apparent from Fig. 4b for the flow field at 2000 m that currents are highly controlled by the topography.

Figure 5a shows the surface flow, and Fig. 5b the flow at 100 m depth during August. At the equator strong currents of about 50 cm s^{-1} are obtained with a well-developed equatorial current, north-equatorial countercurrent, and an undercurrent of 50 cm s^{-1}. Compared with February (Fig. 2) the north-equatorial countercurrent has intensified at the expense of the equatorial current. A narrow band of strong divergence is noticeable at the equator, reflecting enhanced upwelling during the season of stronger trade winds. As in the simulation of Sarmiento (1986, henceforth called S) or Philander and Pacanowski (1986a,b), the seasonally dependent flow patterns near the equator are in good agreement with observations, for example, presented by Richardson and Walsh (1986). However, the model used here seems to be in closer geostrophic balance near the equator than does S. This also corresponds to weaker heat input in the upwelling regions in the present model (see below). This could mean that this model is less diffusive. Indeed, the horizontal diffusion coefficients for momentum, temperature, and salinity are significantly smaller than in S, but a smaller numerical vertical diffusion could also be a factor.

The sea level elevation (Fig. 6) for February reflects these currents. The difference between the highest point off the coast of Florida and the lowest point south and east of Greenland is 1.3 m. Rather strong gradients in

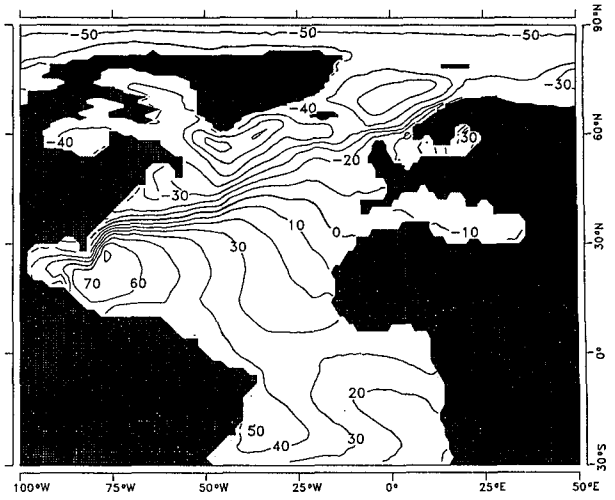

FIG. 6. Surface elevation for February. Contour interval is 10 cm. The thick line denotes the initial mean height of the surface.

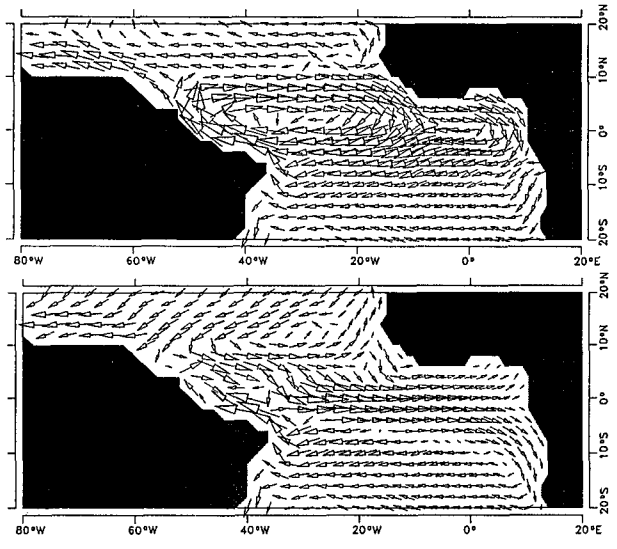

FIG. 5. Upper panel (a) shows the surface flow field and the lower panel (b) the flow at 100-m depth. Cutout of the model domain from 20°S to 20°N. Higher latitudes have nearly identical flow pattern as in Fig. 2; every second vector plotted.

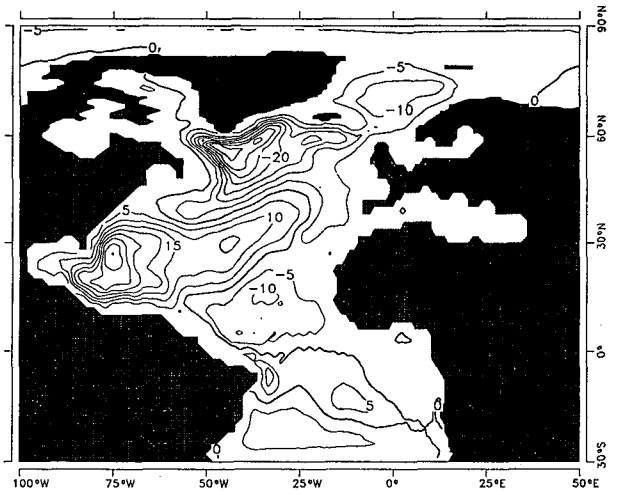

FIG. 7. Horizontal mass transport streamfunction for February in units of 10^9 kg s^{-1} (≡1 Sv). Contour interval is 5 Sv.

the elevation at the North American coast are detected, which tend to continue into the North Atlantic and along the Norwegian coast.

Figure 7 shows the vertically integrated mass transport streamfunction for February. It represents the response to the wind stress curl together with the interaction between the baroclinic flow and the topography. The major gyre is the subtropial gyre east of the North American coast. It extends far eastward, with a maximum transport of 40 Sv (1 Sv $\equiv 10^9$ kg s^{-1}) just off the coast of North America. A cyclonic gyre of about 35 Sv occurs south of Greenland. Another large cyclonic gyre appears north of the equator. This is the result of decreased trade winds on the equator during the northern winter, together with an increased wind-stress curl south of the trade wind maximum in the Northern Hemisphere. It is associated with an eastward barotropic flow along the equator. The barotropic streamfunction for August (Fig. 8) shows a weakened maximum of the subtropical gyre but no significant weakening in the middle of the ocean.

Another useful field to study is the meridional overturning transport streamfunction. The field provides some information on effects such as deep-water formation or equatorial upwelling. Figure 9a shows the February mean overturning. The main features are the two cells south and north of the equator describing the equatorial upwelling. During summer (Fig. 9b), a cell of small meridional extent appears associated with the north-equatorial countercurrent. The southern, counterclockwise rotating cell is stronger in August, while the northern branch is stronger in February. The response is largely due to the seasonal cycle of the trades in both hemispheres. The patterns are similar to S but slightly weaker. Since the Gulf Stream does not propagate strictly from west to east but northeastward, and since the position of the Gulf Stream in the presented

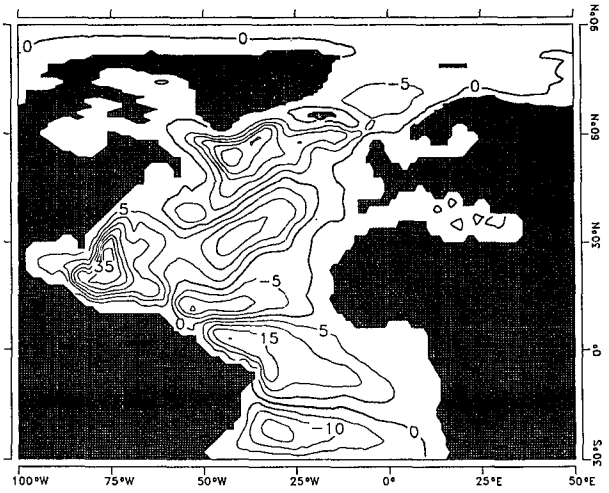

FIG. 8. Horizontal mass transport stream function for August in Sv units. Contour interval is 5 Sv.

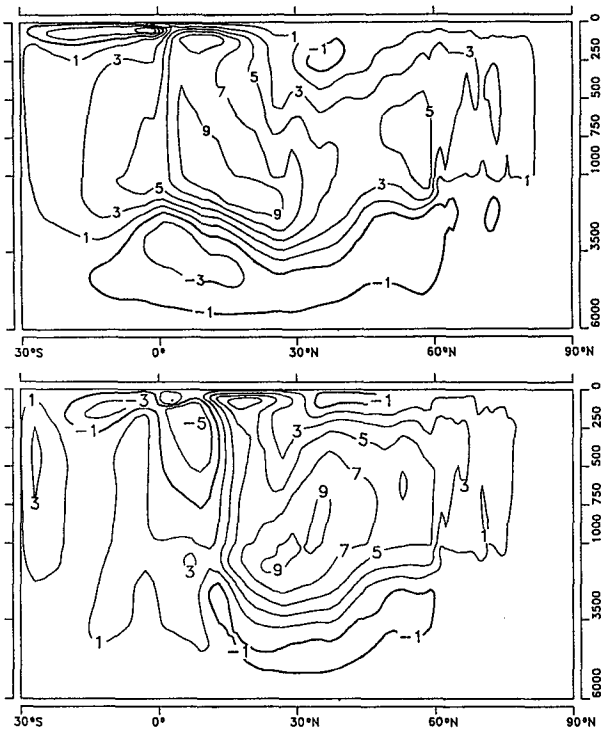

FIG. 9. Upper panel (a) vertical meridional overturning mass transport streamfunction for February. Lower panel (b) vertical meridional mass transport streamfunction for August. In both panels the units are Sv; contour interval is 2 Sv.

simulation differs from that in S, the upwelling and downwelling cancel somewhat differently in the zonal integral. The most significant difference compared with S is that a less strong deep overturning is obtained that extends from high latitudes towards the equator, with a transport slightly higher than 15 Sv at a maximum of 1000 m. This model simulation yields slightly below 10 Sv. This does not imply that the isopycnal model produces less deep water than the z-coordinate model. Mixing processes such as entrainment/detrainment and convection also contribute significantly but do not appear in the meridional overturning (which reflects only the advective part of the transport).

To illustrate how deep water is formed by convection Fig. 10a shows the maximal depth of convection, and Fig. 10b shows the annual mean downward convective potential density flux. The model simulates convection down to 1500 m south of Greenland, and a pronounced maximum with 1300 m appears in the Greenland–Iceland–Norwegian sea area. However, the lowest model layer is not extensively fed by heavy water.

Among the community of ocean modelers it becomes more and more apparent that quantities such as the meridional overturning respond very sensitively even to such details of the external forcing formulation as freshwater fluxes (e.g., river inflow and melting glaciers). In a layer model without vertical mixing, a

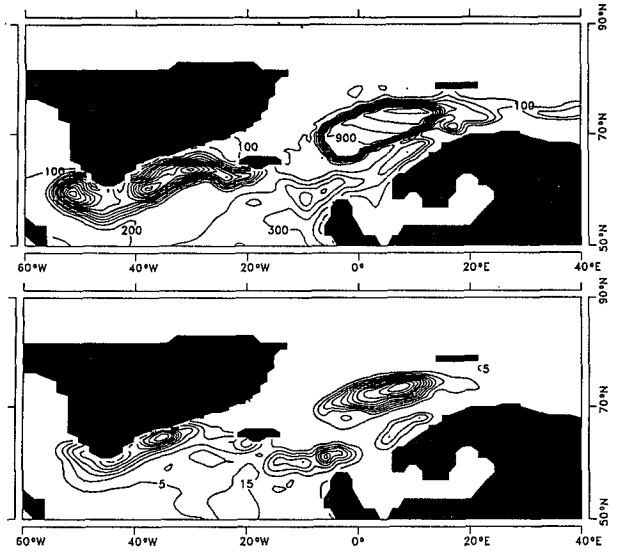

FIG. 10. Upper panel (a) maximal depth of surface convection during the seasonal cycle. Contour interval is 100 m. Lower panel (b) annual mean downward convective potential density flux. Contour interval is 10 kg $(ym^2)^{-1}$.

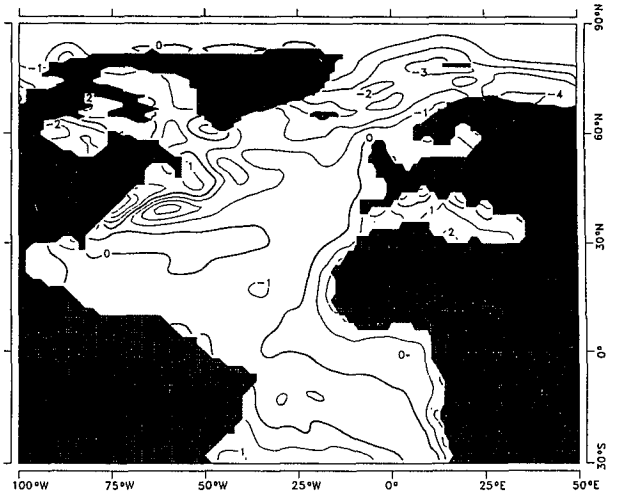

FIG. 11. Annual mean error of the SST. Contour interval is 1 K. Thick line denotes the zero line. The model SST is compared with the SST from COADS. Missing values in the COADS are filled in with the data of Levitus (1982).

strong deep equatorial upwelling, such as that modeled by S, is naturally suppressed in the stationary state, since the Lagrangian coordinates would have to overturn otherwise. A steady vertical mass flux is maintained only by cross-isopycnal mixing, including entrainment/detrainment and convection. Since in this model the Atlantic is a closed basin, the streamlines must also be closed due to mass continuity, whereas in reality most of the deep heavy water produced in the North Atlantic flows into the Indian and Pacific oceans as shown by the Gordon's sketch (1986). In order to obtain a strong meridional overturning the chosen value for $u_* = 5$ mm s^{-1} would have to be increased drastically. Only then could strong deep upwelling be maintained at the equator. But this causes a much too diffusive thermocline in low latitudes. The missing open boundary with prescribed in- and outflow, which is not well known anyway, is a shortcoming in this model layout. It will influence the surface flow into those areas where heavy water descends.

c. *Simulation of surface fluxes*

The present ocean model is forced with an observed atmosphere. The friction velocity u_* needed for evaluating the TKE surface input has no feedback with the ocean state. However, the surface fluxes of heat interact with the SST. The mixed layer depth (MLD) thereby is one important controlling parameter for the upper-ocean response. Typically, the MLD covers values of 10 to 200 m but may extend to 1000 m as in the high-latitude North Atlantic. This induces highly variable response time scales to atmospheric forcing. Since the mixed-layer (ML) model is fully active, coupled to either the interior ocean or to the atmosphere, the sensitivity will be different from that of a model of a surface layer of uniform depth. A further aspect is that the vertical discretization by Lagrangian coordinates yields a quite different view of how heat and salt convergence (the source of any surface flux) work in the subsurface ocean. Therefore, a discussion of the surface fluxes should give some knowledge about how the upper ocean works with Lagrangian coordinates.

1) SURFACE HEAT FLUX

The annual-mean difference between the calculated and the observed SST is shown in Fig. 11 and the an-

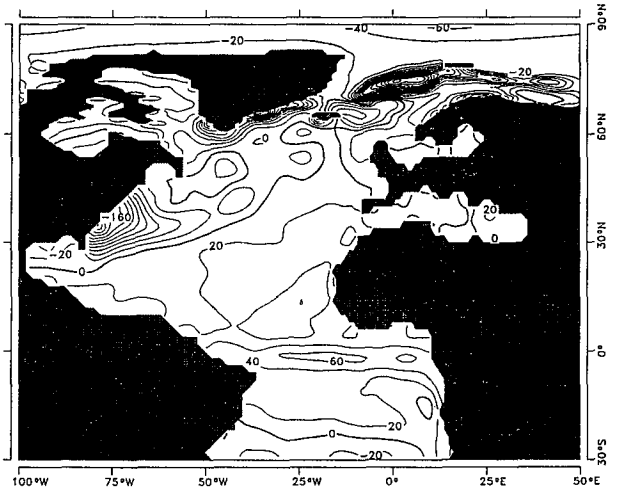

FIG. 12. Annual mean heat flux into the ocean. Contour interval is 20 W m^{-2}. Thick line denotes the zero line.

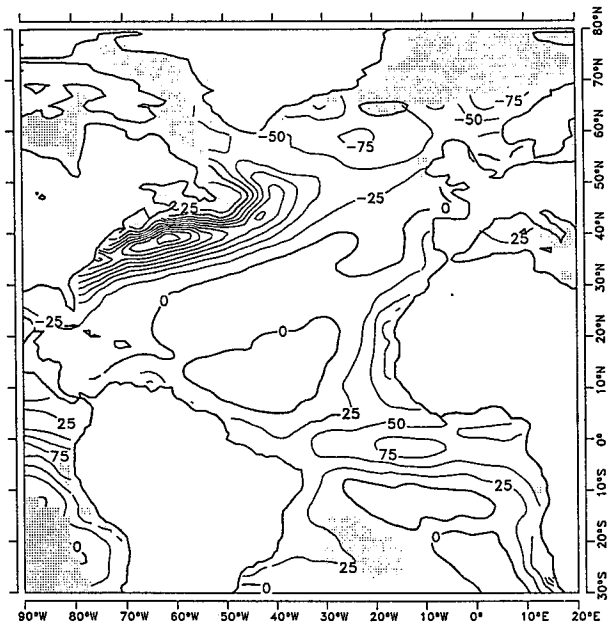

FIG. 13. Annual-mean heat flux analyzed from observed atmospheric quantities taken from the COADS. The contour interval is 25 W m^{-2}. This picture is a cutout of the global fields of the heat flux presented by Oberhuber (1988). Shaded regions in the ocean mark regions of low data quality. The actual coastline is drawn with a thick line.

nual-mean heat flux in Fig. 12. The observed annual-mean heat flux presented in Fig. 13 agrees sufficiently with the model simulation except along the African coast where the forcing temperature is too high due to an interpolation between land and sea points, in the Greenland–Iceland–Norwegian sea area where the SST is typically too low by 2 K and in the Gulf Stream area with errors up to 3 K. At the equator the maximum heat input occurs in the center of the Atlantic. Values of up to 70 W m^{-2} are comparable to those derived from observations. Based on a coarse-resolution observation, Esbensen and Kushnir (1981) and Hsiung (1985, 1986) evaluated the mean heat flux at the equator to be about 50 W m^{-2}. Using a higher resolution dataset, Oberhuber (1988) obtained about 80 W m^{-2}.

In the subtropical South and North Atlantic only two regions of significant heat input occur. They belong to coastal upwelling areas along the South American and North African coasts. In the middle of the ocean the heat flux vanishes. The region of the major heat release appears near the Gulf Stream. The heat loss is about 100–200 W m^{-2} and shows some similarities for the heat flux computation with the COADS (Oberhuber 1988). The differences can be explained by the fact that the Gulf Stream separates slightly too far from the coast—this explains the positive SST error there—and that the Gulf Stream penetrates too far zonally eastward. The resulting SST error of about 2 K explains the differences in the heat flux. It must be added that the errors of individual months are larger, of course. Nonlinearities in the heat flux parameterization due to the dependence of the transfer coefficients on static stability, for example, (this differs quite a lot between summer and winter around Newfoundland) require a month-by-month analysis rather than one based on annual-mean values only.

Sensitivity experiments were carried out with different kinds of atmospheric forcing. It was found that with Newtonian cooling but without an offset through an observed heat flux climatology according to Haney (1971) the Gulf Stream does not separate. From these differences in the behavior of the Gulf Stream and depending on the heat forcing adopted, it appears that a realistic high heat loss is a mechanism that promotes the early separation of the Gulf Stream. A similar effect was found for the freshwater input. A reduced Newtonian damping for salinity yields a reduced north–south salinity gradient due to horizontal advection and diffusion. This can be understood in terms of the generation of a meridional pressure gradient due to a strong gradient of heat loss in the upper ocean. This pressure gradient helps to control the separation of the Gulf Stream. In order to show this effect, a straight coastline was chosen by removing Cape Hatteras. Therefore, the Gulf Stream is not pushed eastward by the coastline, but it separated nevertheless. A further surprising finding during various runs with different ML models is that simulations with a too deep mixed layer north of the Gulf Stream also let the Gulf Stream separate too late. It appears that the Gulf Stream separation responds rather sensitively to the internal structure of the model interfaces and the external forcing. However, the underestimation of the momentum transport through the too slow current speed and that the judgement, whether right or wrong, depends only on a few

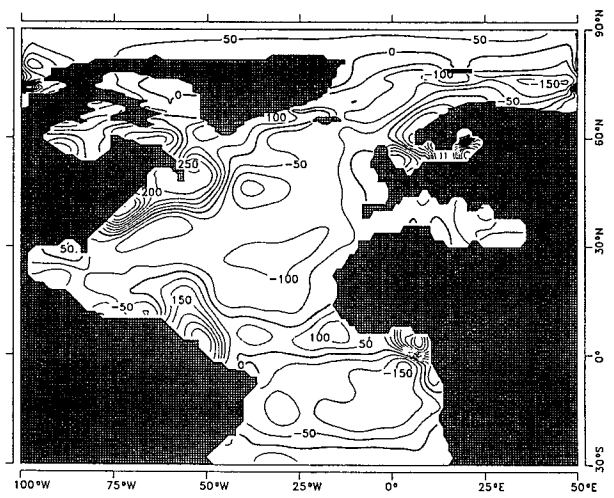

FIG. 14. Annual-mean freshwater flux into the ocean from the model. Contour interval is 50 mm mo^{-1}. The thick line denotes the zero line.

grid cells through the coarse resolution does not allow any final conclusions.

In the simulation carried out by Smith (1987) with the purely wind-driven isopycnal model of Bleck, the Gulf Stream also separates without any thermodynamical forcing. Our interpretation of this result is that due to the missing mixed layer the surface currents have to flow along lines of outcropping isopycnals, with no possibility of moving across these isopycnals in a well-mixed region like the surface layer. In the model used here the Gulf Stream, in principle, has the freedom to propagate in the mixed layer independent of the isopycnal structure. Heat fluxes, therefore, seem to be necessary to control the near-surface flow. In the Greenland–Iceland–Norwegian seas the heat fluxes increase to about 400 W m^{-2}. The vertical convective heat flux in the ocean contributes about 200 W m^{-2} (not shown as a separate quantity), as in the convection area south of Greenland. In polar areas the mean heat flux is small due to the isolation by sea ice.

2) NET FRESHWATER FLUX

The patterns for (P–E) are in some respect more instructive than the heat fluxes. Since P–E has no feedback with the observed values, the results provide indications as to whether the subsurface convergence of salt or more generally of tracers are simulated adequately. Comparing the simulated results (Fig. 14) with analysis of Oberhuber (1988) (Fig. 15) agreement is seen in the (P–E) patterns in the ITCZ and in the subtropical Southern and Northern hemispheres. The amplitudes are realistic and vary between 50–100 mm mo^{-1}. There are two regions, however, that show larger errors. The missing specification of the river inflow due to the Congo and Amazon yields an artificial additional freshwater input. The other error pattern occurs north of the Gulf Stream, where the model obviously has difficulty in keeping the salinity sufficiently low. A net freshwater flux of several hundred millimeters per month is required to maintain the observed salinity. However, the missing freshwater input from the St. Lawrence River partly accounts for the error in the P–E. A surprising aspect of the sea ice–ocean coupling are the P–E values in the Arctic basin, which vary between 0 and 50 mm mo^{-1}. This corresponds to the estimated 25 cm yr^{-1} used by Lemke (1987) to study the response to changed Soviet river inflow. Since the Arctic basin is essentially closed towards lower latitudes, which makes salt transport out of the Arctic basin unimportant, it can be concluded that the sea ice–mixed layer–deep ocean coupling yields a realistic downward salt transport in the annual mean.

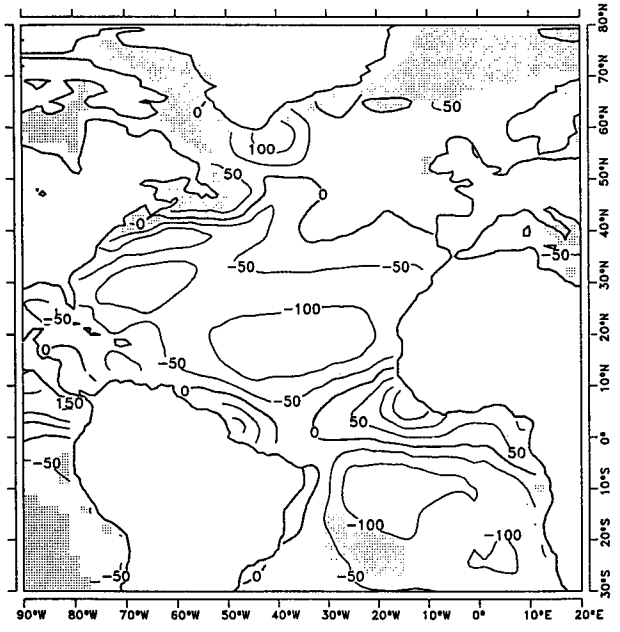

FIG. 15. Annual-mean freshwater flux into the ocean analyzed by taking the rainfall data of Shea (1986) and the evaporation. The contour interval is 50 mm mo^{-1}. The picture is a cutout of the global fields of the net freshwater flux presented by Oberhuber (1988).

d. Mixed-layer simulation

One of the main difficulties with the determination of the MLD is that several quantities can be chosen to assess how deeply the surface layer is well mixed. Basically, the depth is determined by defining the deviation of some quantity to its surface value. Depending on the chosen quantity rather different patterns for the global fields of the MLD are obtained. The most popular methods are to choose a reasonable temperature or potential density difference for evaluating the MLD. The first criterion is more reliable at lower latitudes, whereas potential density differences are more reliable if salinity effects are of importance, as in high latitudes. Regardless of the criterion chosen, there are large uncertainties in analyses of the MLD. This becomes obvious when the MLD derived by Levitus (1982, Figs. 95a,b, 96a,b) are compared with each other for the two described critera or when another study, such as that by Robinson et al. (1979), is considered.

Figure 16 presents the mixed-layer depth for February. Compared with Levitus (1982), the model simulates the major features of the spatial distribution for the winter case. In the eastern part of the equatorial Atlantic a MLD of 20 m is simulated increasing to 50 m towards the west. Coinciding with the trade wind maxima mixed layer depths of 100 m in the Northern Hemisphere and 60 m in the Southern Hemisphere are obtained. This is in good agreement with the patterns obtained by Levitus with the 0.5 K temperature difference criterion. Towards midlatitudes the mixed layer deepens rapidly at about 25°N, typically to 150 m. Both criteria presented by Levitus indicate the existence of a tongue of a deep mixed layer extending from the Florida Current northeastward into high latitudes. The

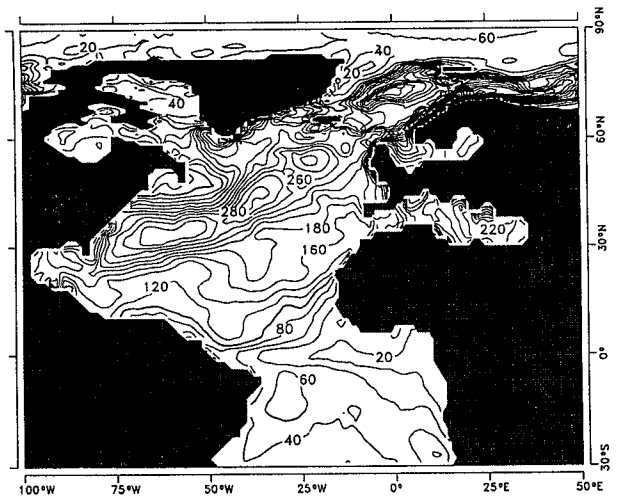

FIG. 16. Thickness of the mixed layer in February. Contour interval is 20 m. The thick line marks a depth of 100 m.

σ_t criterion (0.125 kg m^{-3} difference to the surface density) yields 100 m there. Slightly too small values, down to 300 m south of Iceland, are simulated. The shallow mixed layer south of Newfoundland is evident both in the presented results and the observed data, and there is good agreement between the simulation and the observations in Baffin and Hudson bays. Between Greenland and Labrador the MLD decreases rapidly towards 20 m compared with the σ_t criterion. In contrast to this deep high-latitude ML it becomes rather shallow in the Arctic basin with values of 20–60 m. The reason for this is the realistic salinity stratification and the effect of sea ice in isolating the ML from extreme wintertime atmospheric conditions, thereby making the input of TKE and buoyancy small.

One difference, compared with the analysis by Levitus (1982), appears in the Gulf Stream area. The tongue of a deep ML extends too far towards the Caribbean Sea. An analysis of the near-surface Gulf Stream offers one possible answer. Since the Gulf Stream is too weak due to its insufficient spatial resolution on the 2° × 2° model grid, the northward transport of warm near-surface water is underestimated. Consequently, it is not surprising to find stability too low in the near-surface Gulf Stream as the initial condition for the deepening of the ML during autumn. This error pattern is also supported by the small stability in the thermocline of the subtropical gyre as shown later (Fig. 24a).

Figure 17 shows the MLD at the end of the northern summer. A generally shallow mixed layer of 20–60-m depth exists in the Northern Hemisphere with the deepest extension in the trades. In order to attain this realistic behavior it is important to allow solar radiation to penetrate into the ocean. Otherwise, the buoyancy flux into the ML would be overestimated and the ML would therefore be too shallow.

The annual-mean upwelling rates are presented in Fig. 18. The model simulates the important upwelling areas, such as that at the equator with mean values of about 0.7 m day^{-1}. These upwelling rates are also surprisingly strong in the trades where values of up to 0.5 m day^{-1} appear along the North African coast and at the coast of Venezuela with upwelling rates of about 0.5 m day^{-1}. These entrainment rates are consistent with a narrow band of shallow ML there. The patterns change in the subtropical gyre where downwelling of about 0.1 m day^{-1} is connected with the descending water in the strong anticyclonic flow east of the Gulf Stream. The upwelling rates with values of up to 0.3 m day^{-1} south of Newfoundland correspond to the shallow mixed layer and describe the vertical overturning in the Gulf Stream extension.

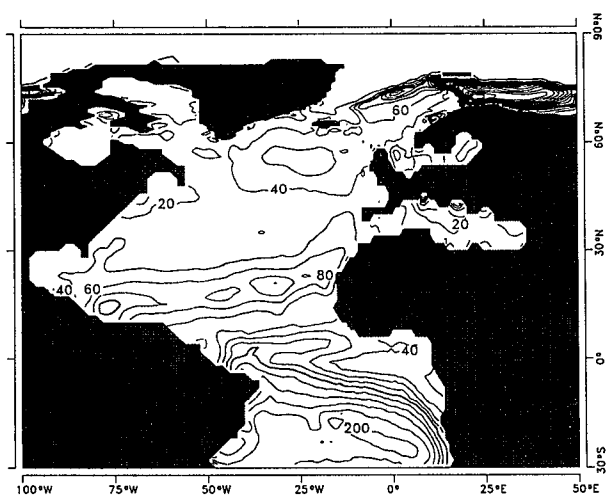

FIG. 17. Thickness of the mixed layer in August. The thick line marks a depth of 100 m.

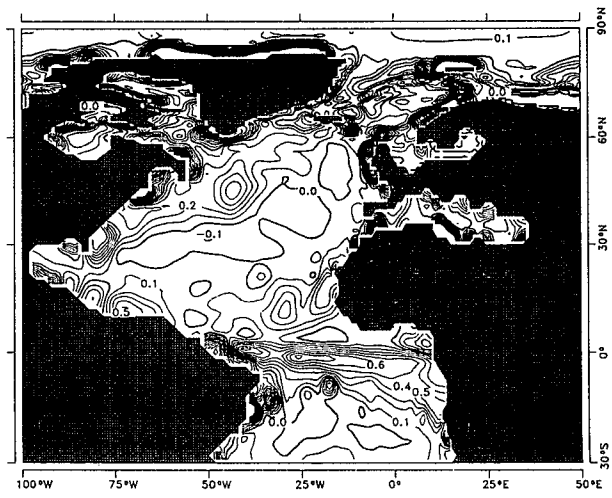

FIG. 18. Annual mean entrainment rate. Contour interval is 10 cm day^{-1}. The thick line denotes the zero line. This field is identical to the field of annual mean upwelling rates in a cyclostationary state.

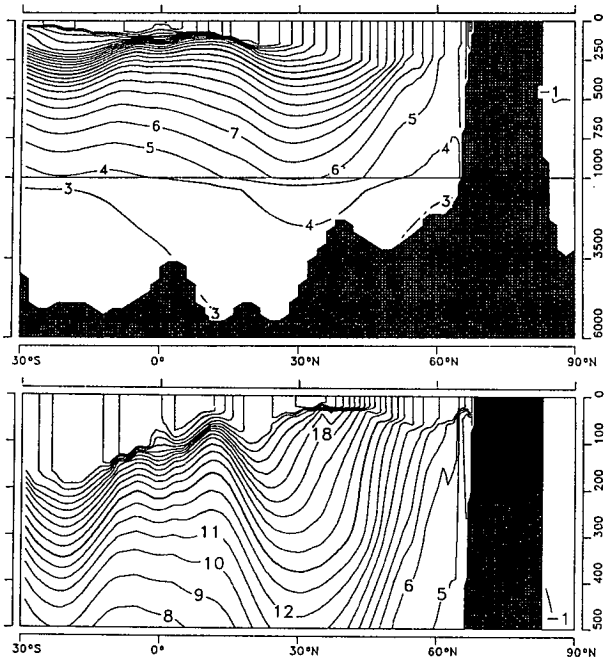

FIG. 19. Meridional cross section of potential temperature at 30°W. Upper panel (a) shows the model prediction for February, and the lower panel (b) shows the model prediction for August for the upper 500 m. Contour interval is 1 K. The thick line denotes the 15°C isotherm.

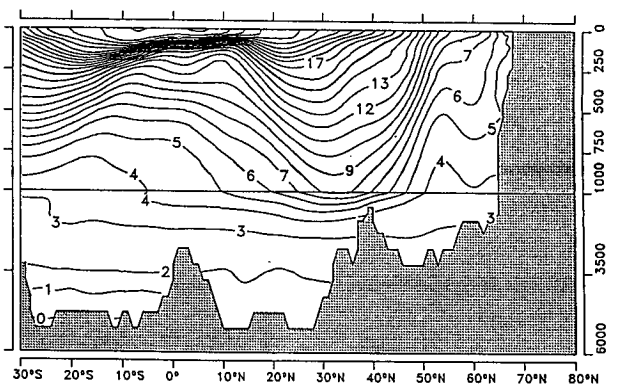

FIG. 20. Meridional cross section of annual mean observed temperature at 30°W taken from the dataset of Levitus (1982). Contour interval is 1 K. The thick line denotes the 15°C isotherm.

e. *Vertical stratification*

The next component of the presented OGCM is the isopycnal coordinate model for the deep ocean. Variations of the MLD due to entrainment/detrainment and convection determine the forcing of the interior ocean. Now the 100-year simulation of the thermocline is discussed by comparing selected cross sections with the observed annual-mean fields prepared by Levitus (1982).

A comparison of the meridional cross section at 30°W for the potential temperature in February (Fig. 19a) with the annual mean observations (Fig. 20) shows a good agreement. The exception is the near-surface boundary layer, in which stratification clearly reflects the effects of winter conditions in the Northern Hemisphere. Both model and observations show a deep thermocline in the subtropics, where downwelling water depresses the isotherms. In contrast, the thermocline is rather sharp in the tropical upwelling regions. This agrees with the annual-mean upwelling rates (Fig. 18). The main difference between the monthly mean field for February and the observed annual mean is the existence of colder surface water in the Northern Hemisphere in the model together with a deep layer of constant temperature due to the mixed layer. In the Southern Hemisphere the situation is reversed. Compared with February (Fig. 19a), the simulation of the August temperature distribution (Fig. 20) exhibits a distinctly shallower mixed layer in the Northern Hemisphere with a significant step in the temperature near the surface. The stratification in the thermocline is unchanged.

The simulation of the salinity for February, shown in Fig. 21a, reproduces the basic observed patterns, with high surface salinities in the subtropics due to net evaporation. The only major difference here is the missing freshwater tongue in the model, which extends from the Southern Hemisphere into the North Atlantic

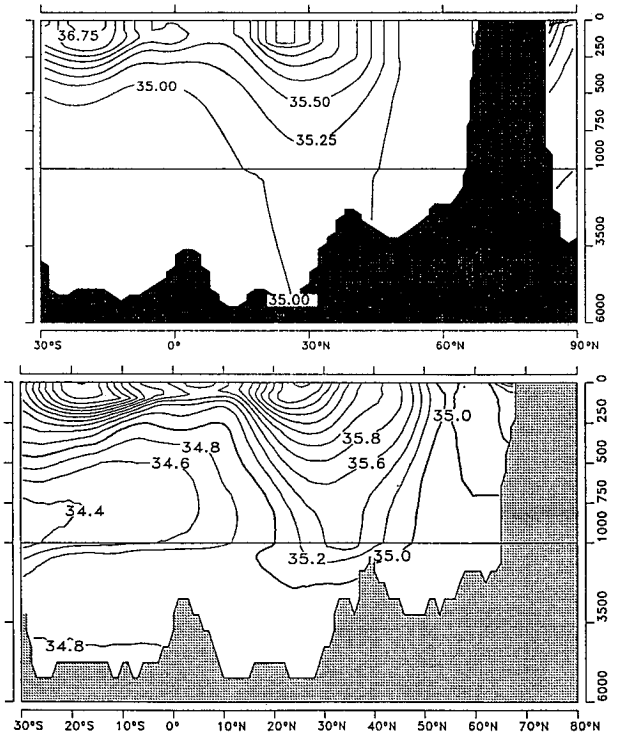

FIG. 21. Meridional cross section of salinity at 30°W. Upper panel (a) shows the model prediction for February and the lower panel (b) shows the annual-mean observation taken from the dataset of Levitus (1982). Contour interval is 0.2 per mille. The thick line denotes the 35 per mille isohaline.

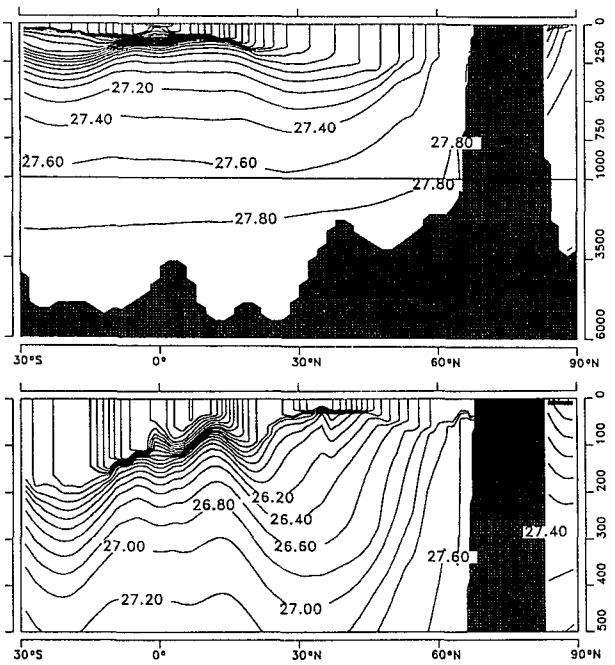

FIG. 22. Meridional cross section of potential density at 30°W. The upper panel (a) shows the model prediction for February and the lower panel (b) shows the model prediction for August for the upper 500 m. Contour interval is 0.2 kg m^{-3}. The thick line denotes the 25 kg m^{-3} isopycnal.

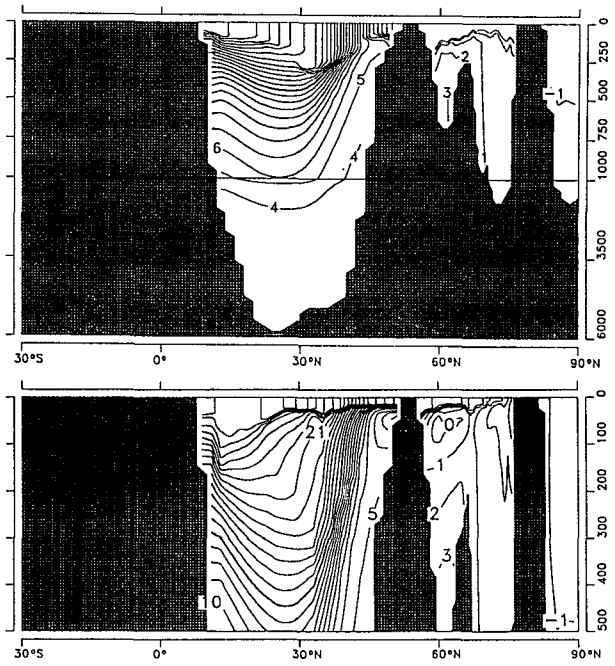

FIG. 24. Meridional cross section of potential temperature at 60°W. The upper panel (a) shows the model prediction for February and the lower panel (b) shows the model prediction for August for the upper 500 m. Contour interval is 1 K. The thick line denotes the 15°C isotherm.

in the observed annual-mean salinity at 30°W (Fig. 21b). Since the model is bounded at 30°S, the northward extent of the Antarctic Intermediate Water at a depth of about 1 km and the cold Antarctic Bottom Water are suppressed. Figures 22a,b present the simulated February, and Fig. 23 the observed annual-mean potential density at 30°W. The effect of the nonlinear equation of state is clearly evident in the much shallower patterns compared to those for the temperature.

The ability of the model to simulate the stratification in the free ocean is evident in further cross sections shown for some critical near-coastal regions. A meridional section at 60°W encompasses the Gulf Stream fronts and upwelling along the coast of Venezuela. Figure 24a shows the potential temperature for this cross section at 60°W for February, Fig. 24b for August, and Fig. 25 the observed annual mean. Figure 26a shows the corresponding salinity cross section for February and Fig. 26b the observed annual mean. The model

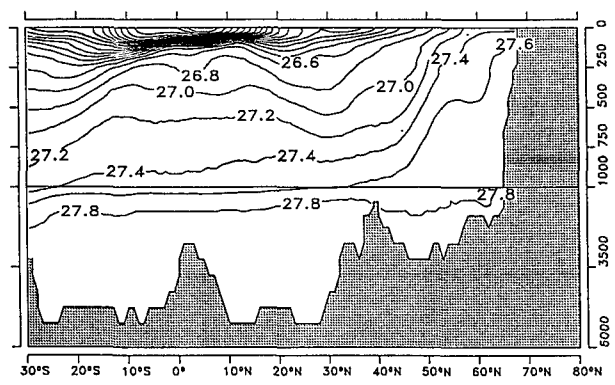

FIG. 23. Meridional cross section of annual mean observed of potential density at 30°W derived from the dataset of Levitus (1982) from temperature and salinity by using the UNESCO formula and defining the surface as reference pressure level. Contour interval is 0.2 kg m^{-3}. The thick line denotes the 25 kg m^{-3} isopycnal.

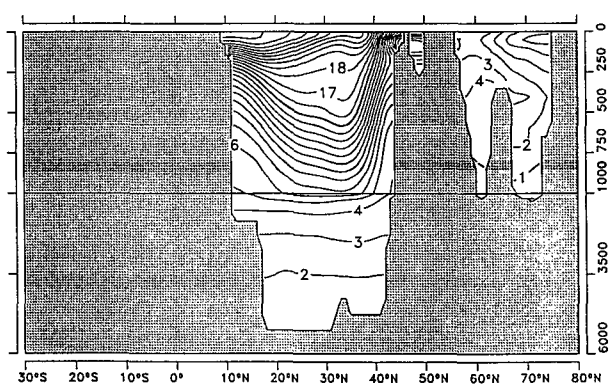

FIG. 25. Meridional cross section of observed annual mean potential temperature at 60°W taken from the dataset of Levitus (1982). Contour interval is 1 K. The thick line denotes the 15°C isotherm.

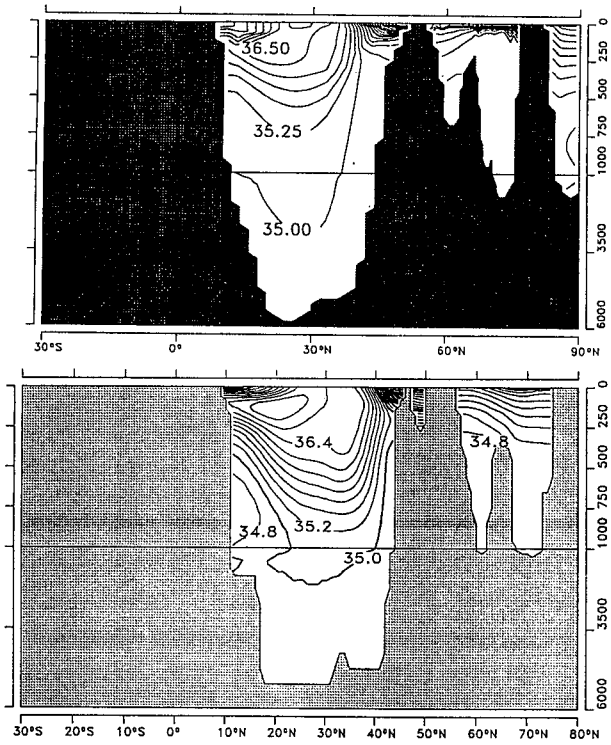

FIG. 26. Meridional cross section of salinity at 60°W. Upper panel (a) shows the model prediction for February and the lower panel (b) shows annual-mean observations taken from the dataset of Levitus (1982). Contour interval is 0.2 per mille. The thick line denotes the 35 per mille isohaline.

has no difficulties in developing a strong front in the temperature and salinity fields around the Gulf Stream despite the coarse resolution. The only apparent discrepancy occurs at a depth of between 200 and 500 m in the subtropical gyre. The observed stratification is rather weak there. It is unclear whether the model's failure to reproduce this feature indicates a deficiency of the transformation from the isopycnal coordinates onto z coordinates for plotting purposes or of the model's physics or is simply the result of the low number of layers.

Until now only cross sections for quantities transformed into z coordinates have been shown. To demonstrate how the solution appears in model coordinates Figs. 27a,b show the coordinate positions for February and August by the meridional cross section at 60°W. Each mass grid cell is marked accordingly by a step (compare with Fig. 7 of Part I). These figures indicate how the interfaces and layers change their role in the upper ocean during the seasonal cycle of the mixed layer and the complexity of the occuring patterns of physically existing and vanishing layers.

In summary, the stratification in the upper ocean as simulated by the isopycnal model is, in general, realistic. The model is capable of maintaining strong vertical subsurface gradients of the subtropical gyres in the tropics and the deep depression of isotherms in downwelling areas in the subtropics. At first, this result seems in conflict with the weak deep overturning. It should be noted that compared to z-coordinate models the model is able to compensate a weaker upwelling by less cross-isopycnal mixing. In the extreme case of no mixing Lagrangian coordinates need no upwelling to maintain their positions. Furthermore, because of the choice of isopycnic coordinates the pressure field is not influenced by alongisopycnal flow. In this model a strong meridional overturning is mainly the response to a steady perturbation of the oceanic pressure field due to mixing processes. Since no artificial mixing is involved in this model, the pressure field is disturbed only by mixing that is caused by the explicitly included parameterizations for vertical mixing. Experiments with a different vertical diffusivity showed a sensitive behavior of the meridional overturning. But it was also found that the stratification is rather robust against changes of any parameterization.

f. Results from the sea ice model

The three basic variables in the sea ice model are ice thickness, ice concentration, and ice velocity. The corresponding pictures for the February mean fields are shown in Figs. 28a,b,c. Since the sea ice extent is largely controlled by the prescribed air temperature and

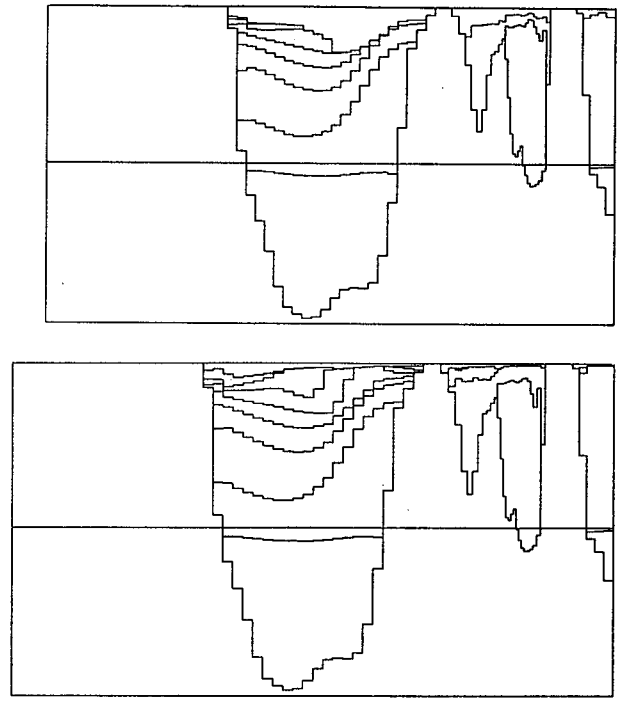

FIG. 27. Meridional cross section of interface distribution at 60°W. The upper panel (a) shows a section for February and the lower panel (b) shows a section for August. Notice that the interfaces are plotted as steps that correspond to Fig. 7b of Part I.

only slightly modified by the ice dynamics, the model simulates the ice edge with reasonable fidelity. The ice thickness in the Davis Strait increases rapidly towards 2.5 m at the northern end of Baffin Bay and extends southward along the Canadian coast towards Newfoundland. This result is in good agreement with the observations of Parkinson et al. (1987). The average sea ice concentration for the years 1973–76 from Parkinson et al. (1987) is modeled adequately. The only significant error is that the sea ice along the west coast of Greenland extends too far south, but this may be due to insufficient resolution of the atmospheric forcing data and ocean currents. In the Arctic basin the interpretation of the results are questionable. Many factors such as a missing whole basin, discretization errors due to the coordinate convergence at the North Pole, and insufficient wind-stress data contribute to an unsatisfactory simulation. The important point to be demonstrated here is that the sea ice model is stable at very small grid distances, which is a precondition to use this model in a global domain.

In the East Greenland Drift, a maximum ice thickness of more than 2 m is attained. In all ice-covered areas the ice concentration (Fig. 29b) is about 95%. The ice concentration decreases rapidly toward the ice margin. The ice flow reflects the role of the Coriolis force. In the Davis Strait the northwesterly winds drive a southward ice flow. This leads to thicker ice at the Canadian coast through ice convergence. The Coriolis force of the northeasterly winds north of Iceland push the ice towards the coast of Greenland, which explains the thick ice of up to 2.5 m in this region. During summer (Fig. 29 a,b,c) the sea ice melts and almost vanishes in Baffin Bay until the end of August. Sea ice of low ice concentration and small thickness remains only in the northernmost part of the Baffin Bay. In the Arctic the sea ice still has about 2-m ice thickness and an ice concentration of about 50%. The model agrees with the observations by Parkinson et al. (1987). They reported such a situation for July and no sea ice for August in Baffin Bay.

In summary, it appears that the thermodynamics and the rheology are adequately treated for this application. This has been verified by Holland et al. (1992) who made extensive sensitivity experiments with this realization of Hibler's viscous–plastic rheology for the entire Arctic basin. Comparing the high sensitivity of the model results with the choice of sea ice parameters, the model seems to be well adjusted and therefore should also work in a global context. For studying the Atlantic circulation only, a useful technique is to enable the model code to work on a grid that is rotated by

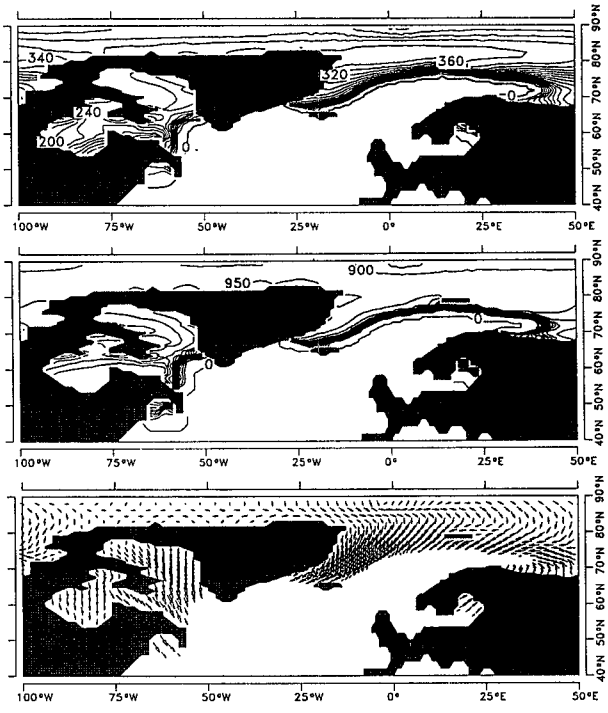

FIG. 28. The upper panel (a) shows the mean ice thickness for February from 40°N to 90°N. Contour interval is 20 cm. The middle panel (b) shows the ice concentration for the same time and latitudes. Contour interval is 5 ppt. The lower panel (c) shows the ice velocity vectors also for the same period and latitudes. Only each second vector is plotted. Typical ice velocities are 10–15 cm s^{-1} at the ice edge and only a few cm s^{-1} in totally ice-covered areas.

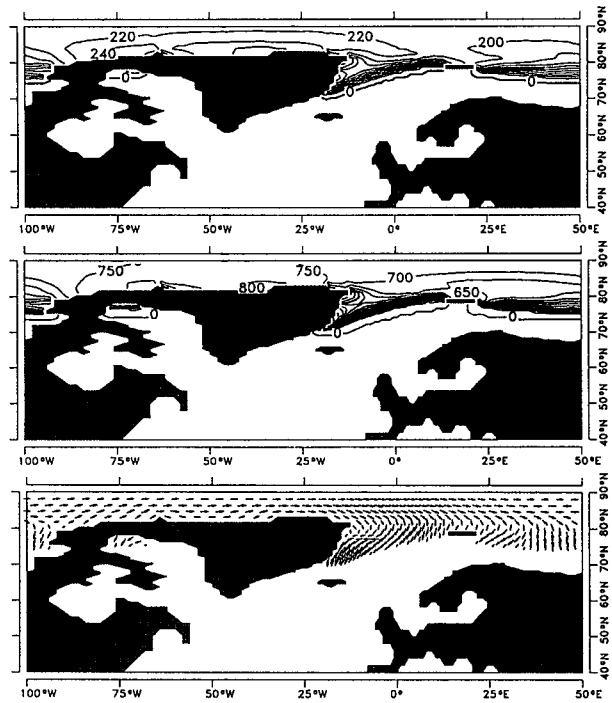

FIG. 29. The upper panel (a) shows the mean ice thickness for August from 40°N to 90°N. Contour interval is 20 cm. The middle panel (b) shows the ice concentration for the same time and latitudes. Here, the contour interval is 5 ppt. The lower panel (c) shows the ice velocity vectors also for the same period and latitudes. Every second vector is plotted.

Eulerian angles. As already successfully tested, the entire Arctic can be connected to the North Atlantic without having a highly converging grid within the model domain, since the model coordinate pole can be positioned in the North Pacific, for instance.

5. Conclusions

The goal of this study was to demonstrate the feasibility of a diabatic circulation model based on isopycnic coordinates and primitive equations coupled to a mixed-layer model and a sea ice model with rheology. The model experiments are carried out for the equatorial and North Atlantic. The OGCM was forced with fluxes that are derived from the COADS. The behavior of the model with climatological seasonal forcing has been investigated. Basic quantities, surface fluxes, the mixed-layer simulation, the vertical stratification, and results from the sea ice model have been discussed.

The model simulates the mean state of the upper ocean satisfactorily. Currents, surface fluxes, and vertical representation of the thermocline are realistically modeled. The mixed-layer model is the result of numerous experiments of various types with such models. With the optimized mixed-layer parameterization the thickness of the surface boundary layer was simulated reasonably well under all conditions, including equatorial upwelling regimes, in the subtropics, in midlatitudes, and below the Arctic sea ice. However, questions remain that to some extent might have their reason in the chosen artificial walls for this limited-area model. One of these questions, for example, concerns the weak meridional overturning in the deep ocean. From the time development of the temperature in the deep ocean it is evident that sufficient deep water is being formed to keep the bottom water at a high potential density, but because of the artificial boundary at 30°S the advective part of the overturning is weak. Deep water cannot flow into the South Atlantic and also cannot easily cross the isopycnals in upwelling areas of the low latitudes. Otherwise, large vertical diffusion coefficients are necessary to allow, for example, 20 Sv upward transport in an area of small horizontal extent as it is the equatorial Atlantic. On the other hand, it cannot be excluded at present that fundamental deficiencies have yet to be removed. This can be clarified only in the context of a global model.

However, the simulated mean state of the thermocline should have demonstrated that the model is already in a state in which it can be used for studies on decadel time scales. While in the past, efforts have concentrated on the major technical problems to realize an ocean model based on isopycnal coordinates, the future must be to understand and correct the model physics. An advantage of this model concept is its completeness: it combines a detailed parameterization of the mixed layer, a sea ice model with rheology, an isopycnal representation of the deep ocean, a realistic equation of state, and allows an arbitrary topography. This is an investment into future applications of this model. The results presented here for a limited-domain version are sufficiently promising to warrant an extension of the model to the global domain and its subsequent use in climate studies.

Acknowledgments. The author would like to thank Professors K. Hasselmann and D. Olbers for initiating this work and especially Professor Hasselmann for reviewing and discussing this paper. Acknowledgment is made to the Deutsches Klimarechenzentrum for providing the large amount of computer times necessary to develop this model and Peter Wright for improving the manuscript. This study was supported by the European Community (EV4C-0035D(B)) and the Bundesminister für Forschung und Technologie (BMFT-KF212/1, BMFT-07KFT05/6).

REFERENCES

Bleck, R., and D. B. Boudra, 1986: Wind-driven spin-up in eddy-resolving ocean models formulated in isopycnic and isobaric coordinates. *J. Geophy. Res.*, **91**, 7611–7621.

Böning, C. W., R. Döscher, and R. G. Budich, 1991: Seasonal transport in the western subtropical North Atlantic: Experiments with an eddy-resolving model. *J. Phys. Oceanogr.*, **21**, 1271–1289.

Bryan, K., 1969: A numerical method for the study of the circulation of the World Ocean. *J. Comput. Phys.*, **4**, 347–376.

Bryan, F. O., and W. R. Holland, 1989: A high resolution simulation of the wind- and thermohaline driven circulation in the North Atlantic Ocean. Proc. 'AhaHuliko'a, Hawaiian Winter Workshop. P. Müller, D. Henderson, Eds., University of Hawaii at Manoa, 99–115.

Cox, M. D., 1984: A primitive equation three-dimensional model of the ocean. GFDL Ocean Group Tech. Rep. No. 1, GFDL/NOAA, Princeton University, Princeton, 250 pp.

Esbensen, S. K., and Y. Kushnir, 1981: The heat budget of the Global Ocean: An atlas based on estimates from surface marine observations. Climate Research Institute, Oregon State University, Rep. No. 29, 27 pp, 188 figs.

Gordon, A. L., 1986: Interocean exchange of thermocline water. *J. Geophys. Res.*, **91**(C4) 5037–5046.

Haney, R. L., 1971: Surface thermal boundary conditions for the ocean circulation models. *J. Phys. Oceanogr.*, **9**, 815–846.

Hellerman, S., and M. Rosenstein, 1983: Normal monthly wind stress over the world ocean with error estimates. *J. Phys. Oceanogr.*, **13**, 1093–1104.

Holland, W. R., and D. Hirschman, 1972: A Numerical calculation of the circulation in the North Atlantic Ocean. *J. Phys. Oceanogr.*, **2**, 336–354.

Holland, D. M., L. A. Mysak, D. D. Manak, and J. M. Oberhuber, 1992: Sensitivity study of a dynamic thermodynamic sea-ice model. *J. Geophys. Res.*, submitted.

Hsiung, J., 1985: Estimates of global oceanic meridional heat transport. *J. Phys. Oceanogr.*, **15**, 1405–1413.

——, 1986: Mean surface energy fluxes over the Global Ocean. *J. Geophys. Res.*, **91**, 10 585–10 606.

Killworth, P. D., D. Stainforth, D. Webb, and S. M. Paterson, 1991: The development of a free-surface Bryan–Cox–Semtner ocean model. *J. Phys. Oceanogr.*, **21**, 1333–1348.

Krauss, W., 1986: The North Atlantic Current. *J. Geophys. Res.*, **91**(C4), 5061–5074.

Lee, W. H. K., and W. M. Kaula, 1967: A spherical harmonic analysis of the earth's topography. *J. Geophys. Res.*, **72**, 753–758.

Lemke, P., 1987: A coupled one-dimensional sea ice–ocean model. *J. Geophys. Res.*, **92**, 13 164–13 172.

Levitus, S., 1982: *Climatological atlas of the World Ocean.* NOAA Prof. Paper No. 13, U.S. Govt. Printing Office, 173 pp., 17 fiche.

McDougal, T. J., and J. A. Church, 1986: Pitfalls with the numerical representation of isopycnal and diapycnal mixing. *J. Phys. Oceanogr.*, **16,** 196–199.

Miller, A. J., J. M. Oberhuber, N. E. Graham, and T. P. Barnett, 1991: Tropical Pacific response to observed winds in a layered general circulation model. *J. Geophys. Res.*, submitted.

Oberhuber, J. M., 1988: An atlas based on the 'COADS' data set: The budgets of heat, buoyancy and turbulent kinetic energy at the surface of the global ocean. Max-Planck-Institut für Meteorologie/Hamburg, Rep. 15, 199 pp.

Oberhuber, J. M., 1993: Simulation of the Atlantic circulation with a coupled sea ice-mixed layer-isopycnal general circulation model. Part I: Model description. *J. Phys. Oceanogr.*, **23,** 808–829.

Olbers, D. J., M. Wenzel, and J. Willebrand, 1985: The inference of North Atlantic circulation patterns from climatological hydrographic data. *Geophys. Rev.*, **23,** 313–356.

——, J. C. Cosimo, H. J. Zwally, D. J. Cavalieri, P. Gloersen, and W. J. Campbell, 1987: Arctic Sea Ice, 1973–1976: Satellite passive-microwave observations. NASA Sp-489, Washington DC. 296 pp.

Philander, S. G. H., and R. C. Pacanowski, 1986a: A model of the seasonal cycle in the tropical Atlantic Ocean. *J. Geophys. Res.*, **91,** 14 192–14 206.

——, and ——, 1986b: The mass and heat budget in a model of the tropical Atlantic. *J. Geophys. Res.*, **91,** 14 212–14 220.

Redi, M. H., 1982: Oceanic isopycnal mixing coordinate rotation. *J. Phys. Oceanogr.*, **12,** 1154–1158.

Richardson, P. L., and D. Walsh, 1986: Mapping climatological seasonal variations of the surface currents in the tropical Atlantic using ship drifts. *J. Geophys. Res.*, **91**(C9), 10 537–10 550.

Robinson, M. K., R. A. Bauer, and E. H. Schroeder, 1979: *Atlas of North Atlantic–Indian Ocean Monthly Mean Temperature and Mean Salinities of the Surface Layer.* U.S. Naval Oceanographic Office Ref. Publ. 18, Washington D.C., 213 pp.

Sarmiento, J. L., 1986: On The North and tropical Atlantic heat balance. *J. Geophys. Res.*, **91,** 677–689.

Shea, D. J., 1986: *Climatological Atlas: 1950–1979,* Surface air temperature, precipitation, sea-level pressure, and sea-surface temperature (45°S–90°N). NCAR Technical Note TN-269+STR, 35 pp.

Smith, L. T., 1987: A wind-driven isopycnic coordinate model of the North and equatorial Atlantic Ocean. Ph.D thesis, University of Miami.

Unesco, 1981: The practical salinity scale 1978 and the International Equation of State of Seawater 1980. UNESCO Tech. Pap. in Mar. Sci., No. 36, 13–21.

Woodruff, S. D., R. J. Slutz, R. L. Jenne, and P. M. Steurer, 1987: A comprehensive ocean-atmosphere data set. *Bull. Amer. Meteor. Soc.*, **68,** 1239–1250.

Wright, P., 1988: An Atlas based on the 'COADS' data set: Fields of mean wind, cloudiness, and humidity at the surface of the Global Ocean. Max-Planck-Institute for Meterology/Hamburg, Report 14, 70 pp.